Inorganic Chemistry

pubs.acs.org/IC

Article

Exploring the Change in Redox Reactivity of UO_2 Induced by Exposure to Oxidants in HCO_3^- Solution

Junyi Li,* Xianjie Liu, and Mats Jonsson

Cite This: *Inorg. Chem.* 2023, 62, 7413−7423

Read Online

ABSTRACT: Understanding the possible change in UO_2 surface reactivity after exposure to oxidants is of key importance when assessing the impact of spent nuclear fuel dissolution on the safety of a repository for spent nuclear fuel. In this work, we have experimentally studied the change in UO_2 reactivity after consecutive exposures to O_2 or γ-radiation in aqueous solutions containing 10 mM HCO_3^-. The experiments show that the reactivity of UO_2 toward O_2 decreases significantly with time in a single exposure. In consecutive exposures, the reactivity also decreases from exposure to exposure. In γ-radiation exposures, the system reaches a steady state and the rate of uranium dissolution becomes governed by the radiolytic production of oxidants. Changes in surface reactivity can therefore not be observed in the irradiated system. The potential surface modification responsible for the change in UO_2 reactivity was studied by XPS and UPS after consecutive exposures to either O_2, H_2O_2, or γ-radiation in 10 mM HCO_3^- solution. The results show that the surfaces were significantly oxidized to a stoichiometric ratio of O/U of $UO_{2.3}$ under all the three exposure conditions. XPS results also show that the surfaces were dominated by U(V) with no observed U(VI). The experiments also show that U(V) is slowly removed from the surface when exposed to anoxic aqueous solutions containing 10 mM HCO_3^-. The UPS results show that the outer ultrathin layer of the surfaces most probably contains a significant amount of U(VI). U(VI) may form upon exposure to air during the rinsing process with water prior to XPS and UPS measurements.

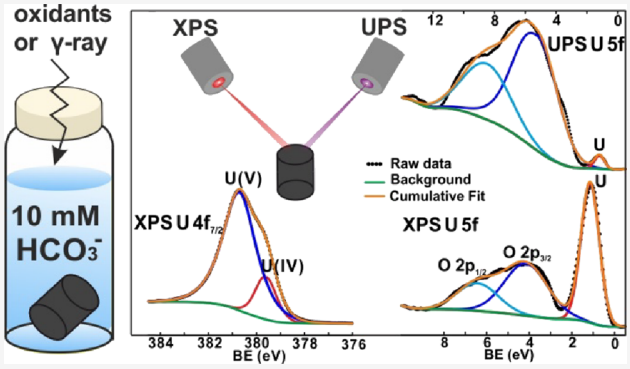

■ INTRODUCTION

Nuclear power is a significant contributor to the total energy supply in many countries. It is regarded as a clean energy source in the sense of CO_2 emissions and therefore has an important impact on sustainable development.[1,2] However, the obvious drawback is the inevitable production of highly radiotoxic spent nuclear fuel. For UO_2-based fuel (the most common type in commercial reactors), the spent nuclear fuel contains approximately 95% UO_2 and 5% radioactive fission products or heavier actinides.[3,4] Since the start of the nuclear power era, more than 400,000 t of spent fuel has been generated. About two-thirds is kept in storage while the other third has been reprocessed.[5] Currently, the spent nuclear fuel is temporarily stored in storage pools or in dry casks. Permanent storage of spent nuclear fuel is an essential component of the nuclear waste management system in several countries. Many countries plan to place the spent nuclear fuel in geological repositories where the hazardous material will be protected by engineered and natural barriers for periods exceeding 100,000 years.[6−10] Given the extremely long time periods during which the repository must remain safe, extensive safety assessments are required before taking a repository into use. Groundwater intrusion is a potential scenario that must be considered. When groundwater comes into contact with the spent nuclear fuel, the radiolysis of water produces both oxidants ($OH^{\cdot}$, H_2O_2, $HO_2^{\cdot}$, and O_2) and reductants (e_{aq}^-, $H^{\cdot}$, and H_2).[11,12] In general, UO_2 has very low solubility in water. However, after the U(IV) is oxidized by the radiolytic oxidants to U(VI), the solubility of the fuel matrix will significantly increase. The solubility is further enhanced by the formation of highly soluble complexes between U(VI) and Lewis base ligands (e.g., CO_3^{2-}, OH^-, O_2^{2-}).[13−16] The concentrations of HCO_3^- in the groundwater with a depth relevant to repositories (ca. 500 m) are in the range 0.1−10 mM.[17−21] The radiation-induced oxidative dissolution of the fuel matrix (UO_2) will result in radionuclide release, and therefore, understanding UO_2 matrix dissolution under repository conditions is of major importance for the safety assessment of a deep geological repository.[22]

In general, at HCO_3^- concentrations as high as 10 mM, the UO_2 surface is assumed to be kept free from oxidized UO_2 and

Received: March 1, 2023
Published: May 2, 2023

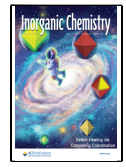

https://doi.org/10.1021/acs.inorgchem.3c00682
Inorg. Chem. 2023, 62, 7413−7423

the stoichiometry is expected to be $UO_{2.0}$. However, in some fairly recent studies of H_2O_2-induced oxidative dissolution of UO_2 pellets in 10 mM HCO_3^-, it was discovered that the redox reactivity of UO_2 decreases with increased H_2O_2 exposure.[23] H_2O_2 has been shown to react with UO_2 via catalytic decomposition to produce O_2 and H_2O and by oxidizing the surface. The observed change in reactivity only applied to the latter reaction pathway. Raman spectroscopy shows that the surface is significantly oxidized after the exposure of H_2O_2 even in solutions with 10 mM HCO_3^-.[23] This implies that there might be a stable (or semi-stable) oxidized phase formed on the UO_2 surface that can alter the redox reactivity of the material. Similar studies for other radiolytic oxidants have not been presented as far as we know.

Torrero et al.[24] studied the dissolution of UO_2 in carbonate-free solution under different O_2 partial pressures. It was shown that there is no significant difference in the steady-state release rate of uranium between exposure to 5% O_2/N_2 and 100% O_2 at pH 8.6 (a pH close to what is expected in 10 mM HCO_3^-). XPS analysis performed on the UO_2 after exposure revealed a relatively high percentage of U(VI) with a stoichiometry close to $UO_{2.6}$ in the solid surface layer. Furthermore, de Pablo et al. studied O_2-induced dissolution of UO_2 in 0.1−50 mM CO_3^{2-}/HCO_3^- medium and concluded that only a contribution from U(IV) can be observed based on the XPS results.[25]

In this work, we have explored how consecutive O_2 and γ-radiation exposures in aqueous solutions containing 10 mM HCO_3^- affect the reactivity of UO_2. The potential surface modification connected to the exposures was analyzed using X-ray photoelectron spectroscopy (XPS) and ultraviolet photoelectron spectroscopy (UPS). For the surface analysis, specimens exposed to either O_2, H_2O_2, or γ-radiation in aqueous solutions containing 10 mM HCO_3^- were used. The XPS and UPS results were analyzed using the following methods: (1) deconvolution of U $4f_{7/2}$ peak; (2) energy difference between the U $4f_{5/2}$ peak and its corresponding satellite peaks; (3) peak center and FWHM of the O 1s peak; (4) peak area ratio between O $2p_{3/2}$ and U 5f.[26−30] The observed impact of exposure on the reactivity of UO_2 is discussed in view of the XPS and UPS results.

■ EXPERIMENTAL SECTION

Caution! Although the radioactivity of natural uranium (prior to its use in a nuclear reactor) is low, safety precautions regarding work with radioactive materials should be followed. Experiments involving uranium should only be conducted by trained staff and take place in facilities appropriate for the handling.

All solutions were prepared using Milli-Q water (18.2 MΩ cm), and all chemicals used were of reagent grade unless otherwise stated. Hydrogen peroxide 30% (Merck) and sodium bicarbonate ($NaHCO_3$, Merck) were used to prepare stock solutions. The UO_2 pellets (geometrical surface area of approximately 352 mm^2) were supplied by Westinghouse AB.[22]

The concentrations of U(VI) in solution were measured spectrophotometrically using the Arsenazo III method,[31] where uranyl reacts with the Arsenazo III reagent forming a complex in acid media. The absorbance of the complex is measured at λ = 653 nm using a Thermo Scientific Genesys 20 spectrophotometer. During the measurement, 1.5 mL of diluted sample was mixed with 60 μL of 1 M HCl and 40 μL of 16 wt % Arsenazo-III reagent in a cuvette. The detection limit of U(VI) is 0.22 μM.

UO_2 Pellet Surface Pre-Washing. Before the dissolution experiments, the UO_2 pellets were washed in de-aerated 10 mM $NaHCO_3$ to remove the pre-oxidized phase. The washing steps were carried out according to following procedures: Each UO_2 pellet was first rinsed with 10 mM $NaHCO_3$, and then the pellet was placed in a glass vessel with several glass pearls on the bottom of the vessel. Then, 35 mL of 10 mM $NaHCO_3$ was added into the glass vessel and sealed by a rubber septum with N_2 purging for 20 min. The bicarbonate solution was then replaced, and the purging continued for 24 h. After that, the solution was replaced again and the purging continued for 20 min in fresh bicarbonate solution. After washing, the solution was replaced by 40 mL of 10 mM $NaHCO_3$ to be used in the dissolution experiments.

Consecutive O_2 Exposure Experiments. One washed UO_2 pellet with 40 mL of 10 mM $NaHCO_3$ was placed in a glass vessel sealed by a rubber septum. Several glass pearls were placed on the bottom of the glass vessel to increase the surface area of the UO_2 pellet exposed to the solution. The O_2 gas was continuously purged into the solution through a thin glass tube. Three consecutive O_2 exposure experiments were performed at room temperature, and each exposure lasted for 360 h or more. The concentration of U(VI) was monitored as a function of time. For each U(VI) measurement, a 0.8 mL aliquot was taken from the solution. Since O_2 purging can accelerate the evaporation of water, the volume of the solution was recorded after each sampling for further volume compensation calculations. Between individual exposures, the exposed pellet was washed by 10 mM $NaHCO_3$ according to the washing procedure described above.

Consecutive Irradiation Exposure Experiment. For each experiment, one washed UO_2 pellet with 40 mL of 10 mM $NaHCO_3$ and several glass pearls were sealed by a rubber septum in a glass vessel. γ-radiation is emitted from a Cs-137 gamma source (Gammacell 1000 Elite, MDS Nordion) with a dose rate of 0.11 Gy s^{-1} determined by Fricke dosimetry.[11] The sample was exposed to γ-radiation at room temperature for three consecutive times. The concentration of U(VI) was monitored as a function of time. For each U(VI) measurement, 2 mL aliquots were taken from the solution. Before the exposure and after each sampling, the solution was purged with N_2 for 15 min to remove gaseous radiolysis products and then sealed tightly with septum and parafilm. Between individual exposures, the exposed pellet was washed with 10 mM $NaHCO_3$ according to the washing procedure described above. Table 1 summarizes the exposure conditions of the UO_2 pellets used in the dissolution experiments.

Table 1. Summary of the Exposure Conditions of UO_2 Pellets Used in the Experiments

UO_2 pellet	exposure conditions
UP-1	4 O_2 exposures
UP-2	3 γ-irradiation exposures
UP-3	2 O_2 exposures +2 γ-irradiation exposures
UP-4	3 O_2 exposures +2 γ-irradiation exposures
UP-5	3 O_2 exposures +2 γ-irradiation exposures

XPS and UPS. The XPS and UPS experiments were carried out in an ultrahigh vacuum surface analysis system (base pressure of 5×10^{-10} mbar) with a SCIENTA ESCA200 hemispherical electron analyzer. The electrons were excited by a monochromatized Al Kα source (1486.6 eV) for XPS measurements and a standard He discharge lamp He II (40.8 eV) source for UPS measurements. The spectrometer was calibrated with the reference of the Fermi edge (0.0 eV) and Au $4f_{7/2}$ peak position (84.0 eV). The total energy resolution of XPS was set so that the FWHM (full width at half-maximum) of the clean Au $4f_{7/2}$ line (at the binding energy of 84.00 eV) is 0.65 eV. The total energy resolution of UPS was about 0.1 eV, as estimated from the width of the Fermi level. All spectra were recorded at normal emission and room temperature.

Note that the samples used in the XPS measurements were not the same samples used in the dissolution experiments. The samples used in the XPS measurements were UO_2 slices cut from one UO_2 pellet. This was done to minimize the initial difference between the samples and have samples that fit the instrument. This original UO_2 pellet was

https://doi.org/10.1021/acs.inorgchem.3c00682
Inorg. Chem. 2023, 62, 7413−7423

sintered in the same batch as the pellets used in the dissolution experiments. The cut UO_2 slices were exposed to different oxidizing conditions by repeating the procedures described for the dissolution experiments presented above. The exposure details are listed in Table 2. Prior to XPS/UPS analysis, the samples were rinsed with pure water and dried in a glovebox. During the transport from glove box to spectrometers, the samples were sealed in microcentrifuge tubes (Polypropylene) filled with Ar from the glovebox.

Table 2. Samples Used in XPS and UPS and Exposure Conditions Prior to the Measurements

UO_2 slices	exposure conditions before XPS characterizations
US − O_2 ref	stored in a glovebox for a total of 45 days
US − O_2 exp	3 O_2 exposures for a total of 45 days
US − H_2O_2 ref	Stored in glove box for a total of 30 days
US − H_2O_2 exp	3 H_2O_2 exposures for a total of 30 days irradiation
US − irradiation ref	stored in a glovebox for a total of 10 days
US − irradiation exp	3 γ-irradiation exposures for a total of 10 days

XPS and UPS Analysis. Data mining for the XPS and UPS raw data was performed by Thermo Avantage Software (ver. 5.9931). The background was subtracted based on the "smart" function in the software. This "smart" background subtraction is based on the Shirley background subtraction with the additional constraint that the background intensity should never exceed the raw data intensity at any range. The raw data was smoothed by Savitzky−Golay filtering with a window size of 1 eV and polynomial of 4. Peak deconvolution was based on the Gaussian−Lorentzian product function. Specific principles of U 4f, O 1s, O 2p, and U 5f peak deconvolution are described in their corresponding results part.

■ RESULTS

Uranium Dissolution. Figure 1a−e shows the dissolution of uranium from five individual UO_2 pellets consecutively exposed to oxidizing conditions in 10 mM $NaHCO_3$. Each measurement of the U(VI) concentration was performed in a doublet. The average number of the two measured U(VI) concentrations was used in Figure 1. The standard deviation of the two measurements is less than 0.5 μM, and error bars are included in Figure 1. The oxidizing conditions were achieved through exposure to O_2 and γ-radiation in various combinations. Since the solution volume in the reaction vessel will gradually decrease due to sampling and evaporation of water, volume compensated concentrations (normalization) are used throughout the work. Details of the normalization are shown in the Supporting Information.

Figure 1a shows the dissolution behavior of the UO_2 pellet (UP-1) in 10 mM $NaHCO_3$ under 4 consecutive O_2 exposures. The O_2 exposure is achieved by continuously purging the solution with O_2. In this type of exposure, the concentration of O_2 in solution is constant (approximately 1.22 mM determined by Henry's law at 1 atm pressure[32]). Hence, if the reactivity of O_2 toward UO_2 remains constant, we would expect a constant rate of dissolution as long as there are no solubility limitations. As can be seen, within every single exposure, the uranyl concentration increases with exposure time. However, the dissolution slows down with exposure time. It is important to note that the concentrations are still very low compared to the solubility limit of U(VI) under the present conditions. When comparing the consecutive exposures, it is evident that the rate of oxidative dissolution also decreases for each exposure although the initial rate of oxidative dissolution of subsequent exposures is significantly higher than the final rate in the previous exposure. The rationale for this is probably that the surface is altered in a way that reduces the redox reactivity, but that this alteration is at least partly reversible through the washing step between exposures. The same trend was observed also for UP-3−5 during the O_2 exposures. The change in reactivity of the UO_2 pellets can be due to an oxidative alteration of the surface. Figure 1b shows the dissolution of uranium from a UO_2 pellet in 10 mM $NaHCO_3$ under 3 consecutive exposures to γ-radiation. In this system, a number of different one- and two-electron oxidants are formed. The

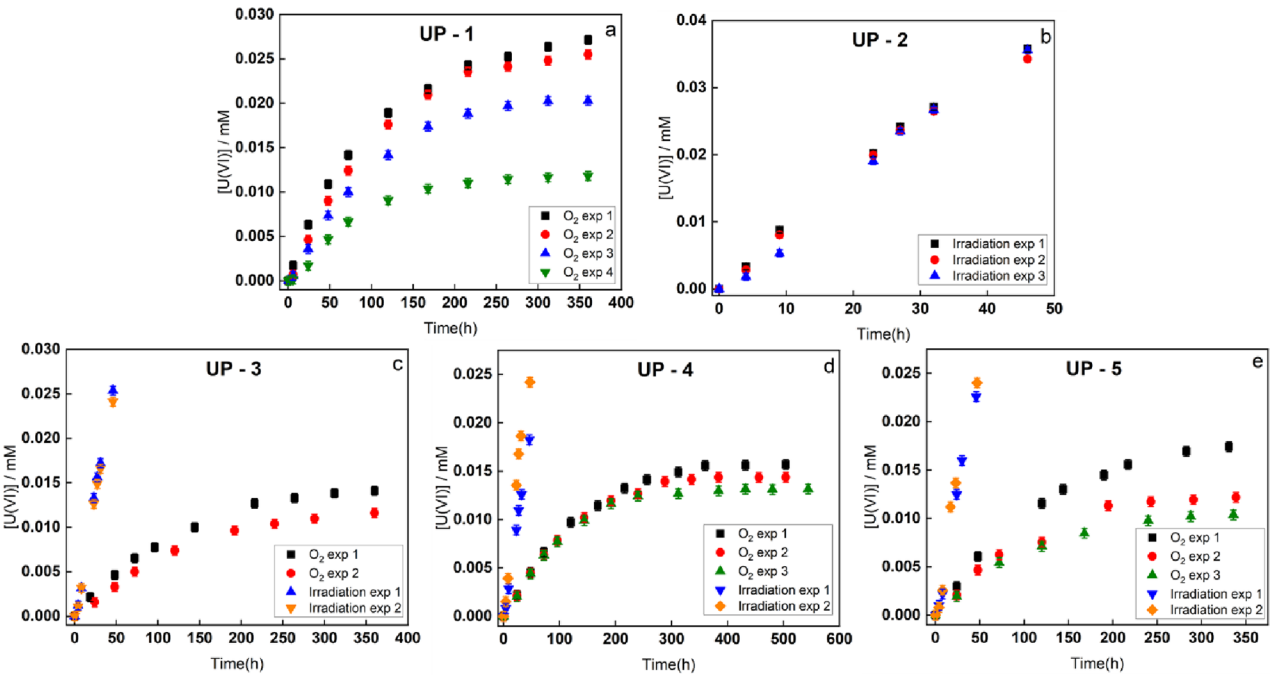

Figure 1. Concentration of U(VI) as a function of time in solutions containing UO_2 pellets in 10 mM $NaHCO_3$ exposed to O_2 or γ-radiation.

https://doi.org/10.1021/acs.inorgchem.3c00682
Inorg. Chem. 2023, 62, 7413−7423

main oxidants are $OH^{\bullet}$, $CO_3^{\bullet-}$ (produced upon reaction between $OH^{\bullet}$ and HCO_3^-), and H_2O_2. These oxidants can oxidize U(IV) to U(V) or U(VI). As can be seen, the uranium concentration increases linearly with irradiation time and the trend is more or less identical for consecutive exposures. The radiation exposures presented for UP-3−5 reveal the same trend. Given the results for O_2 exposure presented above and the previously published results on H_2O_2 exposure,[23] the results for consecutive radiation exposures are somewhat unexpected. However, it should be kept in mind that the exposures to O_2 and γ-radiation are quite different. In the O_2 exposure experiments, the O_2 concentration of approximately 1.22 mM (determined by Henry's law at 1 atm pressure) is maintained constant through the continuous purging with O_2. Any change in rate of oxidative dissolution must then be attributed to a change in the reactivity of the UO_2 surface. During exposure to γ-radiation in a γ-source with a constant dose rate, the rate of oxidant production is constant. In such a system, a steady state will be reached where the rate of oxidant production is equal to the rate of oxidant consumption. If the surface reactivity changes in this system, the steady-state concentration of the oxidants will change until the rate of oxidant consumption is again equal to the rate of radiolytic oxidant production. Hence, we cannot expect to observe a difference in dissolution behavior even if there is a change in surface reactivity.

XPS and UPS. The potential change in oxidation state of UO_2 pellet slice surfaces after three consecutive exposures to either O_2, H_2O_2, or γ-radiation was studied by XPS. Reference samples for each exposure condition were stored in 10 mM $NaHCO_3$ in a glovebox ($O_2 \leq 0.1$ ppm) for the same duration of time as the respective exposures.

Figure 2 shows the narrow scans of U 4f. As can be seen, the measured U $4f_{7/2}$ and U $4f_{5/2}$ in the reference samples are close

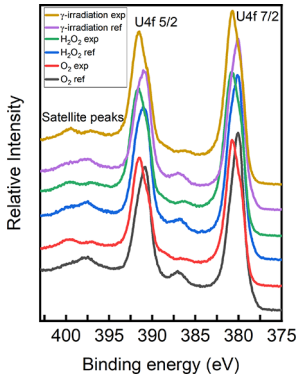

Figure 2. U 4f XPS spectra of the UO_2 slices exposed to various oxidizing conditions and reference samples.

to 380.0 and 391.0 eV, respectively, which is in line with previous results.[26,27,29] Both peaks shift to higher binding energy after exposure to O_2, H_2O_2, or γ-radiation, indicating that the surface was oxidized. There are four methods that can indicate oxidation states of uranium from XPS spectra: (1) deconvolution of the U $4f_{7/2}$ peak; (2) distance between the U $4f_{5/2}$ peak and its corresponding satellite peaks; (3) peak center and FWHM of the O 1s peak; and (4) peak area ratio between O $2p_{3/2}$ and U 5f.[26−30] The present work will utilize all four methods to investigate the oxidation state of uranium. Note that only method 1 was used for quantitative analysis.

Deconvolution Principle. The spectral features of the U $4f_{5/2}$ and U $4f_{7/2}$ core level lines are very sensitive to probe the chemical state of uranium. Since the shape of U $4f_{5/2}$ peaks is affected by the satellite peaks generated from U $4f_{7/2}$ peaks, deconvolution was only performed for U $4f_{7/2}$ peaks. Each U $4f_{7/2}$ peak was assumed to contain three components including U(IV), U(V), and U(VI).[29,30,33] The peak positions in the U $4f_{7/2}$ peak deconvolution process were chosen on the basis of the peak positions of pure U(IV), U(V), and U(VI) materials. The deconvolution principle for mixed valence oxidized UO_2 samples is according to the guidance in ref 34, in which a fixed Gaussian−Lorentzian characteristic, one variable but identical FWHM for each component peak, and a floating peak center is suggested. In this work, a 20% Gaussian−Lorentzian characteristic was used for all U 4f peaks deconvolution, which is similar to the ratio used in ref 35 (15%).[35] FWHM values of U(IV), U(V), and U(VI) peaks in oxidized UO_2 samples were all fixed to 1.40 eV, which is the same as the value used in ref 36. Generally, the peak centers of component peaks are directly related to the chemical environment in XPS spectra. Since the chemical environments (the number of oxygen bond to uranium, and the crystal structure) of U(IV), U(V), and U(VI) can change upon oxidation, the peak centers of U(IV), U(V), and U(VI) were allowed to float close to reference reported values, i.e., ∼380 U(IV), ∼381 U(V), and ∼382 eV U(VI).[33−36] Also, the peak center distance between U(IV) and U(V) was fixed to 1.00 ± 0.02 eV. No U(VI) peak close to 382 eV can be identified by the software (Avantage, ver. 5.9931) in all the U 4f spectra. Examples of forcibly adding the U(VI) peak in the U 4f peak deconvolution was shown and discussed in detail in the Supporting Information (Figure S7). The absence of U(VI) can be attributed to the fairly high HCO_3^- concentrations used in the exposures and the fact that the samples were carefully rinsed with pure water prior to XPS analysis. The cumulative fits are shown in individual deconvolution spectra.

Figure 3 shows the deconvolution of U $4f_{7/2}$ peaks of samples exposed to O_2, H_2O_2, or γ-radiation compared to their corresponding reference samples. The deconvoluted U(IV) peak is marked in red and the U(V) peak is marked in blue. It is clear that the peak area of U(V) increases after exposure. By calculating the peak area ratio between U(V) and U(IV), the stoichiometric ratio of O/U can be obtained. Interestingly, the calculated stoichiometric ratio of O/U of the samples after exposures to all the three oxidizing conditions is close to $UO_{2.32}$. The uranium peak assignment in the U $4f_{7/2}$ spectra in this work is in line with refs 37−39 that reported that the uranium on a $UO_{2.33}$ surface is a combination of U(IV) and U(V) without U(VI). The peak positions, FWHM of the component U(IV) and U(V) peaks, and the calculated peak area ratio between U(V) and U(IV) are summarized in Table 3. The percents of different states of uranium are shown in Table S1.

The U $4f_{5/2}$ peak positions and the positions of its satellite peaks as well as the distance between the U $4f_{5/2}$ peak and its corresponding satellite peaks are summarized in Table 4. The distance between the U $4f_{5/2}$ peak and its corresponding satellite peaks indicates the oxidation states of uranium. In the O_2 exposure reference sample, the distance is 6.65 eV, which is close to the reported value of U(IV) (6.9 ± 0.2).[29] Note that there is another inconspicuous satellite peak in the H_2O_2 and radiation exposure reference samples with the distance toward the U $4f_{5/2}$ peak close to 8.45 eV, indicating that U(V) is

https://doi.org/10.1021/acs.inorgchem.3c00682
Inorg. Chem. 2023, 62, 7413−7423

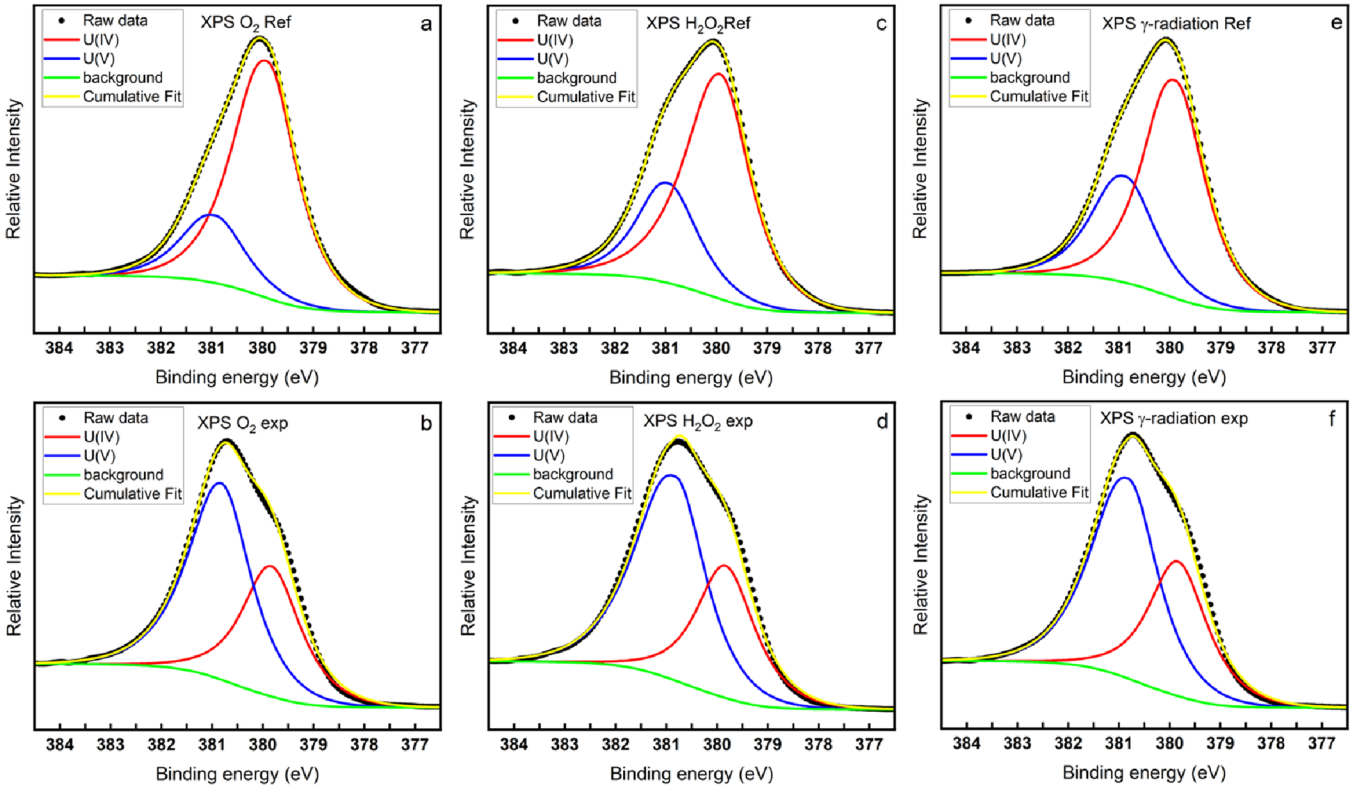

Figure 3. Deconvolution of U $4f_{7/2}$ into U(IV) $4f_{7/2}$ and U(V) $4f_{7/2}$.

Table 3. Summary of the Deconvolution of U $4f_{7/2}$ and the Calculated Stoichiometric Ratio of O/U

exposure condition	U(IV) peak position	U(V) peak position	U(IV) FWHM	U(V) FWHM	area ratio between U(IV) and U(V)	calculated stoichiometry
O_2 ref	379.91	380.93	1.40	1.40	3.55	$UO_{2.11}$
O_2 exp	379.84	380.82	1.40	1.40	0.62	$UO_{2.31}$
H_2O_2 ref	379.92	380.94	1.40	1.40	2.44	$UO_{2.15}$
H_2O_2 exp	379.84	380.82	1.40	1.40	0.55	$UO_{2.32}$
irradiation ref	379.89	380.87	1.40	1.40	2.03	$UO_{2.17}$
irradiation exp	379.84	380.82	1.40	1.40	0.6	$UO_{2.31}$

Table 4. Summary of the U $4f_{5/2}$ Peak Position and the Distance between U $4f_{5/2}$ and the Satellite Peaks

exposure condition	U4 $f_{5/2}$ peak position (eV)	satellite peak (S1) position (eV)	satellite peak (S2) position (eV)	distance between U $4f_{5/2}$ and S1 (eV)	distance between U $4f_{5/2}$ and S2 (eV)
O_2 ref	390.80	397.45		6.65	
O_2 exp	391.45	397.00	399.60	5.55	8.15
H_2O_2 ref	391.10	397.50	399.85	6.40	8.75
H_2O_2 exp	391.55	397.20	399.45	5.65	7.90
irradiation ref	391.05	397.50	399.50	6.45	8.45
irradiation exp	391.50	397.20	399.45	5.70	7.95

present. Moreover, the reported U $4f_{5/2}$-satellite distance value for pure U_2O_5 is 7.9 eV.[26] There are two satellite peaks observed in the O_2, H_2O_2, and radiation exposed samples, with the U $4f_{5/2}$−satellite distance of approximately 5.6 ± 0.15 and 7.95 ± 0.2 eV. The peak with lower binding energy is the U(IV) satellite peak and the other peak with higher binding energy is the U(V) satellite peak. Noteworthily, the satellite peak with higher binding energy is more pronounced than the other satellite peak, indicating the dominance of U(V). The close peak position of the more intense satellite peaks between the oxidized samples indicates the close stoichiometric ratio of O/U. The U $4f_{5/2}$−satellite distances for U(VI) are at 4.4 and 9.9 eV, respectively.[26] As can be seen, these satellite peaks are not present in any of the samples indicating the absence of U(VI) in all the measured samples.

Full XPS scans of US 1−6 were performed, and the spectra are shown in the Supporting Information (Figures S1−S6). The full scan measurements show that only U, O, and C elements are on the surface.

Uranium peroxide ((meta)-studtite) or hydroxide minerals ((meta)-schoepite) are common secondary phases formed on the UO_2 surface.[38,40,41] H_2O_2-induced oxidation through addition of H_2O_2 and water radiolysis generating H_2O_2 could potentially form (meta)-studtite or (meta)-schoepite with oxidized uranium. To elucidate the possible formation of these phases, narrow scans of O 1s spectra were performed on the UO_2 surfaces after the exposures to oxidizing conditions. The results are shown in Figure 4. As can be seen, three peaks can be obtained from the deconvolution of the original O 1s peak. In the reference samples, the peaks are located at approximately, 530.1, 531.4, and 532.7 eV, with an FWHM

https://doi.org/10.1021/acs.inorgchem.3c00682
Inorg. Chem. 2023, 62, 7413−7423

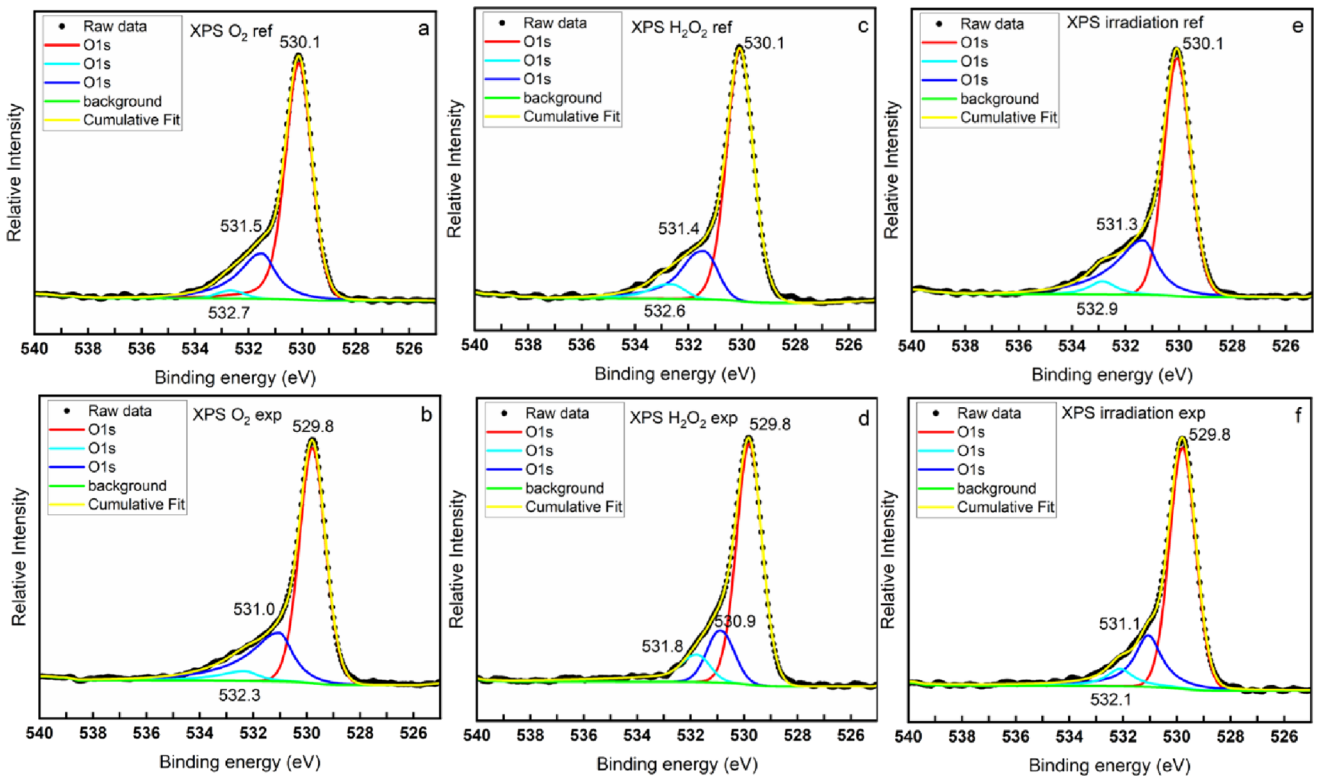

Figure 4. O 1s spectra of the UO_2 slices exposed to various oxidizing conditions and reference samples with the deconvolution of the O 1s peak.

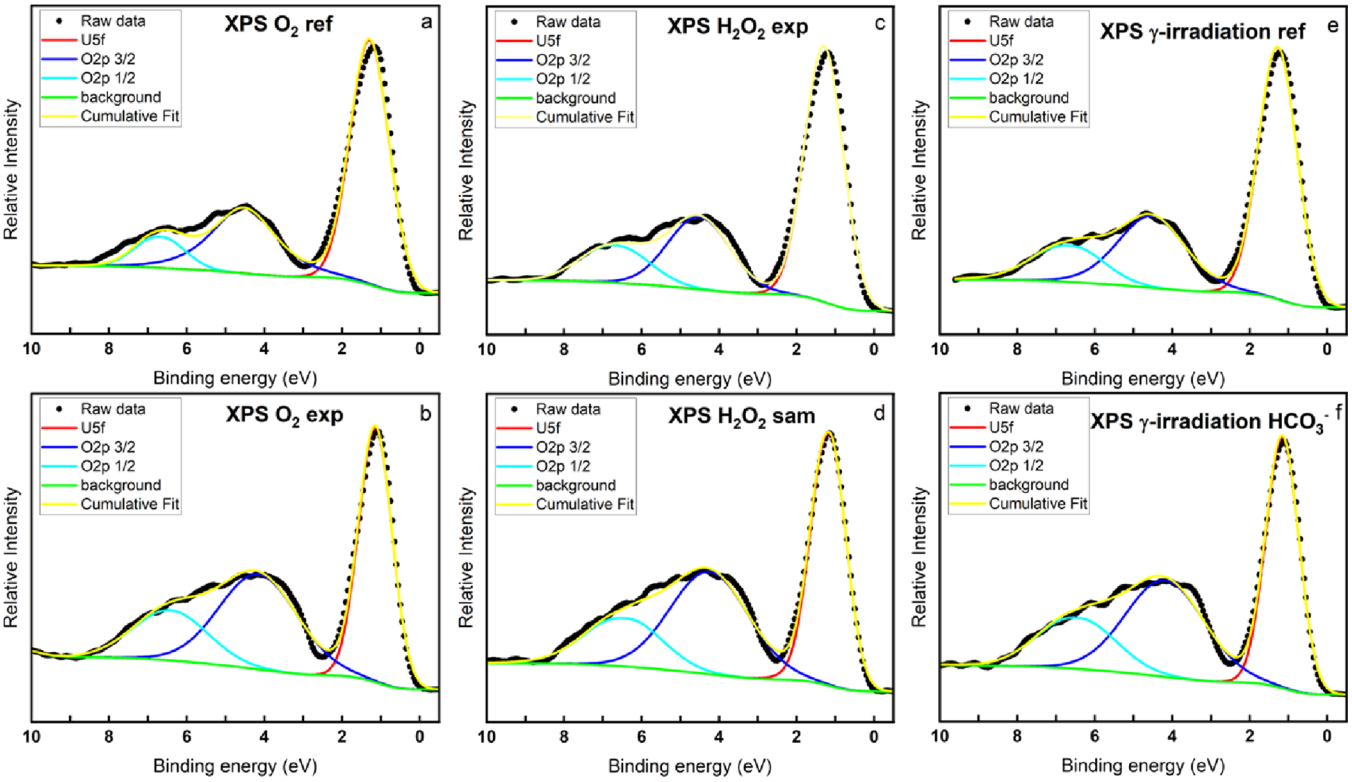

Figure 5. Valence band XPS spectra of the UO_2 slices exposed to various oxidizing conditions and reference samples.

of 1.2 ± 0.03 eV. The peaks at 530.1 eV are narrow in all cases and can be attributed to the oxygen in uranium oxides. The other two peaks have lower intensity and can be attributed to the hydroxyl group (531.4 eV) and carbonate group (532.7 eV). The carbonate group may come from the remaining experimental solution (10 mM HCO_3^-) that was not washed out during the rinsing process.[27] Noteworthily, the CO_3^{2-} peak is not observed in samples leached in solutions free from HCO_3^- (not shown here). The O 1s peaks shift to lower binding energies (529.8, 531.0 ± 0.1, and 532.0 ± 0.3 eV) after

https://doi.org/10.1021/acs.inorgchem.3c00682
Inorg. Chem. 2023, 62, 7413−7423

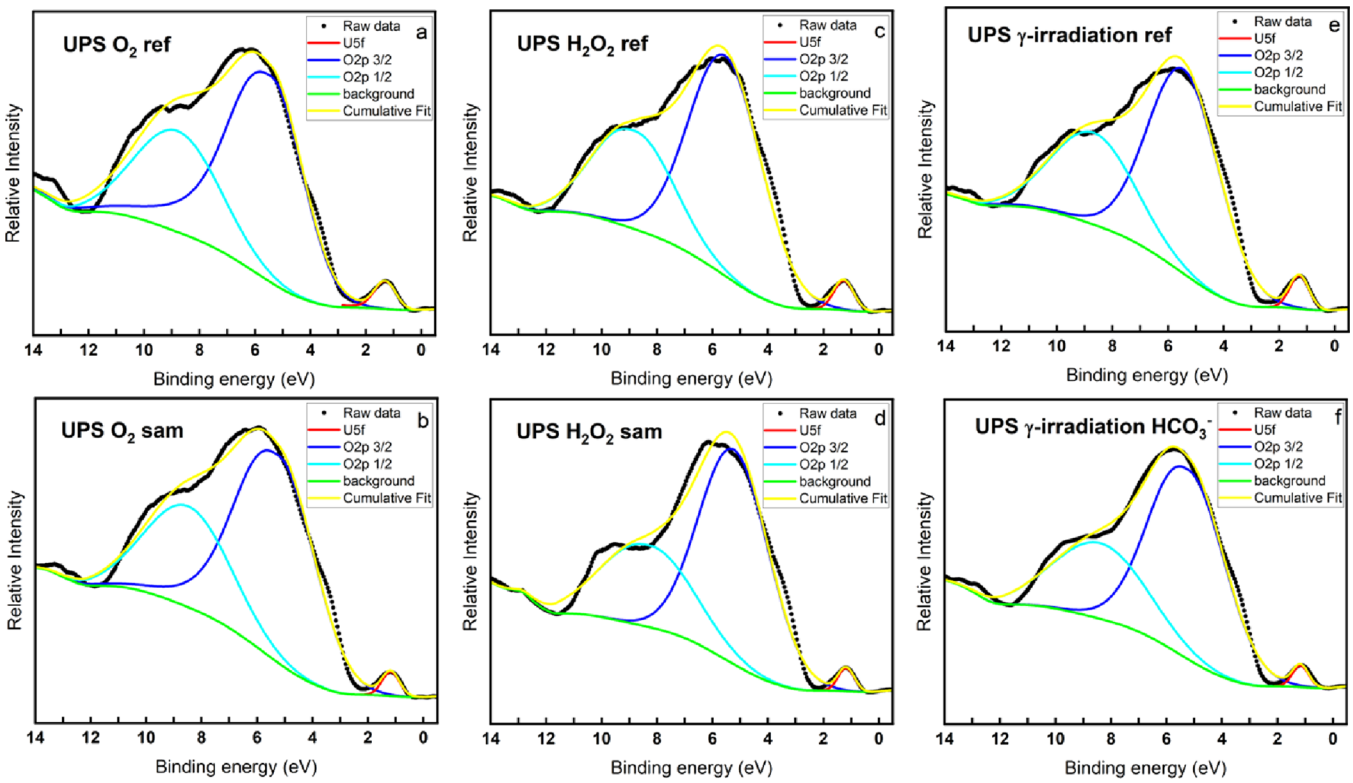

Figure 6. Valence band UPS spectra of the UO_2 slices exposed to various oxidizing conditions and reference samples.

exposure to oxidizing conditions with almost unchanged FWHM (1.2 ± 0.03 eV). The shift of the peaks indicates that the chemical environment surrounding the O atom is significantly changed upon oxidation from U(IV) to U(V). Interestingly, the narrow peaks, under all three exposure conditions, shift to 529.8 eV, representing a close stoichiometric ratio of O/U to each other. Comparing the shape of the narrow peaks at around 530 eV to the much broader O 1s peaks of uranyl peroxides reported in ref 42, formation of peroxide secondary phases can be ruled out. Generally, formation of peroxide or hydroxide secondary phases would lead to increased FWHM and changed peak positions due to the different chemical environment of the oxygen and the difference in crystal structure between the secondary phases and the oxidized UO_2.[42] So far, it is clear that the reduction in redox reactivity of a UO_2 pellet (shown in Figure 1) is not due to formation of peroxide or hydroxide secondary phases but most probably due to the accumulation of U(V) on the UO_2 surface.

Figures 5 and 6 show the XPS and UPS measurements of the U 5f region (0−12 eV). Generally, XPS with an Al Kα source penetrates to a depth of approximately 10 nm (5 layers), whereas UPS with a He II source penetrates to a depth of approximately 1−2 nm (1 layer). In the figures, the sharp peaks at about 1.5 eV are the U 5f peaks. The electronic configuration of uranium in U(IV), U(V), and U(VI) are [Rn]$5f^2$, [Rn]$5f^1$, and [Rn]5f, respectively; therefore, when UO_2 (U(IV)) is oxidized to U(V), the XPS and UPS spectra will display a decrease of the peak area of the U 5f peak. Also, no U 5f peak will be detected for pure U(VI) compounds. The broader peaks at 2−8 eV are the O $2p_{1/2}$ and O $2p_{3/2}$ peaks, the O $2p_{3/2}$ peak is at lower binding energy. The deconvolution is according to the principle that the peak area of O $2p_{3/2}$ should be twice as large as that of O 2p $_{1/2}$ (corresponding to the spin-orbit splitting principle and 2 electrons in the $2p_{1/2}$ level, whereas 4 electrons in the $2p_{3/2}$ level).

It is worth mentioning that the O $2p_{1/2}$ and O $2p_{3/2}$ orbitals can hybridize with the U 6d and U 7s orbitals.[26,43,44] Admittedly, accurate deconvolution and assignment of broad O 2p peaks into O $2p_{1/2}$ and O $2p_{3/2}$ and their hybridization (with U 6d and U 7s) peak are almost impossible due to the lack of relevant references. Since this work focuses on U(IV) to U(VI) oxidation states and there are no U 6d and U 7s electrons in uranium at oxidation states IV−VI, we only deconvoluted the broad O 2p peak to O $2p_{1/2}$ and O $2p_{3/2}$ peaks without taking the peaks for hybridization orbitals into account. In addition, the O 2p peaks for hydroxide and carbonate were not included in the peak deconvolution due to the lack of relevant references. The high FWHM values of O $2p_{1/2}$ and O $2p_{3/2}$ peaks and the poor match between the cumulative fit and raw data can most likely be attributed to the orbital hybridization effect mentioned above and the influence of the O 2p signal from OH^- and CO_3^{2-} groups.

The area ratio of the U 5f peak to the O $2p_{3/2}$ peak is used to compare the oxidation states between the samples. The peak center, FWHM, and peak area of the deconvoluted peaks in the valence band UPS and XPS spectra as well as the area ratio between the U 5f peak and the O $2p_{3/2}$ peak are listed in Table 5. As can be seen, in both the XPS and UPS figures, the decreased area ratio of the samples exposed to oxidants compared to the corresponding reference samples indicates an increased oxidation state of the uranium. The decreased FWHM in the samples exposed to oxidants also indicates an increased oxidation state, and the narrowing of the U 5f peak is due to the change in the population of the U 5f orbital (U $5f^2$ to U $5f^1$ upon U(IV) oxidation to U(V)).[26] Interestingly, the peak area ratio between U 5f and O $2p_{3/2}$ in all the UPS

https://doi.org/10.1021/acs.inorgchem.3c00682
Inorg. Chem. 2023, 62, 7413−7423

Table 5. Summary of the U 5f Peak Position and the Deconvolution of O 2p as Well as the Area Ratio of U 5f and O $2p_{3/2}$

exposure condition	U 5f peak position	O $2p_{3/2}$ peak position	U 5f FWHM	O $2p_{3/2}$ FWHM	area ratio of U 5f to O $2p_{3/2}$
XPS O_2 ref	1.29	4.52	1.18	2.02	3.73
XPS O_2 exp	1.14	4.15	1.01	2.45	1.13
XPS H_2O_2 ref	1.30	4.51	1.18	1.93	2.20
XPS H_2O_2 exp	1.16	4.25	1.02	2.44	1.10
XPS irradiation ref	1.28	4.53	1.17	2.16	1.94
XPS irradiation HCO_3^-	1.16	4.18	1.01	2.46	1.08
UPS O_2 ref	1.30	5.42	0.89	2.70	0.072
UPS O_2 exp	1.18	5.20	0.75	3.00	0.025
UPS H_2O_2 ref	1.26	5.54	0.84	3.13	0.036
UPS H_2O_2 exp	1.17	5.23	0.68	2.96	0.025
UPS irradiation ref	1.27	5.44	0.82	3.05	0.043
UPS irradiation HCO_3^-	1.17	5.20	0.69	3.1	0.024

measurements is almost two orders of magnitude smaller than in the XPS measurements. Considering that the hyperstoichiometric $UO_{2.3}$ obtained from the XPS U 4f deconvolutions is already close to pure U(V), only a combination of U(IV) and U(V) cannot reach such a small ratio between U 5f and O $2p_{3/2}$. Therefore, it is reasonable to assume that an ultrathin layer of the exposed pellets contains a significant amount of U(VI). Table 5 summarizes the FWHM and peak positions of the component U 5f, O $2p_{3/2}$, and O $2p_{1/2}$ peaks and the calculated peak area ratio between U 5f and O $2p_{3/2}$ for both XPS and UPS measurements.

Based on the XPS results presented above, it is clear that the surfaces of the UO_2 samples after exposure to oxidizing conditions in 10 mM HCO_3^- are dominated by U(V) and without measurable amounts of U(VI). Numerous studies using electrochemical methods combined with surface characterization techniques such as XPS have demonstrated that, upon oxidation of UO_2 in aqueous solution, the surface will first be oxidized to a $U^{IV}{}_{1-2x}U^{V}{}_{2x}O_{2+x}$ layer followed by further oxidation to U(VI). Depending on the uranyl-complexing ability of the anions in solution, U(VI) will either deposit on the UO_{2+x} surface or dissolve.[45−52] XPS results in these studies show that when HCO_3^- is present, the oxidized surface was effectively U(V) with negligible amounts of U(VI). The latter being soluble is uranyl carbonate complexes. This is in line with our results i.e., formation of a $U^{IV}{}_{1-2x}U^{V}{}_{2x}O_{2+x}$ layer with U(VI) dissolving in 10 mM HCO_3^- leaching solution. In addition, Ulrich et al.[53] investigated the stability of UO_2 in 1 mM HCO_3^- solution with dissolved oxygen (equilibrium with air). XPS results show that the surface layer contains 20% U(IV), 20% U(V), and 60% U(VI) after exposure. Interestingly, they also observed surface passivation of UO_{2+x} toward oxidative dissolution by O_2 in carbonate solution. Again, the surface passivation as well as the presence of U(V) on the oxidized UO_2 surface are in line with our observations. However, we did not observe the presence of U(VI) on the surface using XPS. This can most likely be attributed to the fact that, prior to XPS analysis, we rinsed the oxidized UO_2 samples with pure water to remove soluble ions and complexes. In the work by Ulrich et al., the samples were dried in an airtight container without rinsing in pure water. Hansson et al.[29] studied UO_2 pellets exposed to radiation in aqueous solution under an Ar atmosphere for 45 days. XPS revealed that UO_2 was oxidized to $UO_{2.33}$ with no identified U(VI).

Exposure to HCO_3^- under Anoxic Conditions. Since UO_2 will be oxidized to hyper-stoichiometric UO_{2+x} by atmospheric O_2 during the dry storage prior to performing the experiments, the pellets and pellet slices were washed in HCO_3^- solutions to remove oxidized uranium. In this work, there are three reference samples stored in 10 mM HCO_3^- in a glovebox ($O_2 \leq 0.1$ ppm) for 45, 30, and 10 days, respectively. The storage time was determined by the exposure time to the oxidizing conditions of the corresponding experiment. The XPS measurements of the reference samples can provide some interesting information about the stability of oxidized UO_2 in 10 mM HCO_3^- solutions. As can be seen from Table 3, the calculated stoichiometric ratio of O/U of the reference samples is $UO_{2.11}$ for the pellet slice exposed to 10 mM HCO_3^- solution for 45 days, and $UO_{2.15}$ and $UO_{2.17}$ for the pellet slices exposed to the same solution for 30 and 10 days, respectively. The UPS data for these specimens indicate that the ultrathin layer of the reference samples is significantly oxidized. Since the oxidation of the ultrathin layer may very well occur during the rinsing of the pellet slice under ambient atmosphere or when transporting the pellet to the instrument for analysis, the actual oxidation state at the end of the exposure to 10 mM HCO_3^- solution could be lower. The findings presented above imply that washing of a hyperstoichiometric uranium oxide surface to stoichiometric UO_2 in anoxic 10 mM HCO_3^- solution can take a substantial time. Hansson et al.[29] also proposed that washing a hyperstoichiometric UO_2 pellet in HCO_3^- to a stoichiometry of $UO_{2.0}$ is a slow process. This is quite interesting when revisiting some fairly recent work showing that a UO_2 surface passivation phenomenon occurs after consecutive exposures to H_2O_2 in 10 mM HCO_3^- solution.[23] This passivation was suggested to be attributed to irreversible alteration of the pellet surface. However, it should be noted that the time to wash the pellet in 10 mM HCO_3^- solution between exposures (24 h) was much shorter than the exposure times discussed above. It is therefore reasonable to suggest that the observed passivation to oxidative dissolution may not be irreversible. The recovery of the exposed surface upon exposure to 10 mM HCO_3^- solution is only slow. The key question here is what the actual mechanism for dissolution of oxidized UO_2 is. According to the XPS data presented above, the dominant form of oxidized uranium on the surface after exposure to oxidants is U(V). To the best of our knowledge, there are no reports on direct interactions between U(V) and HCO_3^-/CO_3^{2-} or on direct dissolution of U(V). It has been shown that U(V) is a state within the fluorite lattice with charge compensation by interstitial O, while U(VI) usually forms a layered structure.[37,57,58] Hence, the oxidation of U(V) to U(VI) involves a significant structural rearrangement, which probably has a direct impact on the kinetics of the process. U(V) is known to undergo disproportionation to produce U(IV) and U(VI) in solution.[54−56] If this reaction is also possible on a solid surface (as has been proposed by

https://doi.org/10.1021/acs.inorgchem.3c00682
Inorg. Chem. 2023, 62, 7413−7423

Ulrich et al.[53]), this might explain why oxidized UO_2 is slowly removed from the surface in the absence of an oxidant (i.e., U(VI) is removed once it is formed). The high proportion of U(V) on the surface and the slow reduction in U(V) content upon exposure to HCO_3^- solution under anoxic conditions demonstrate the kinetic inertia of the process. It is interesting to note that in experiments where pure U(V) phases (U_2O_5) have been produced by reducing U(VI) (UO_3), both the U(V) and the U(VI) phases have layered structures and reduction of U(V) to U(IV) involves a structural rearrangement. This structural rearrangement is also expressed in terms of kinetic inertia of the process.[30] This deserves to be studied in more detail.

■ CONCLUSIONS

The change in UO_2 reactivity after consecutive exposures to either O_2 or γ-radiation was studied. It was shown that the reactivity of UO_2 decreased during O_2 exposure in 10 mM HCO_3^-. The passivation phenomenon could not be observed for γ-radiation exposures since the system reaches a steady state. The surface of UO_2 exposed to oxidizing conditions (O_2, H_2O_2, and γ-radiation) in 10 mM HCO_3^- was characterized by XPS and UPS. The XPS results show that the surfaces were significantly oxidized and dominated by U(V). Quantitative analysis was performed based on the deconvolution of the U $4f_{7/2}$ peak, and the stoichiometric ratio of O/U of the oxidized surfaces was calculated to $UO_{2.3}$ for all the three oxidizing conditions. XPS measurements do not reveal any U(VI) on the exposed surfaces. However, UPS measurements indicate that the outer ultrathin layer contains a significant fraction of U(VI). Exposing the UO_2 pellets to anoxic aqueous solutions containing 10 mM HCO_3^- efficiently removes U(VI), while removal of U(V) is a much slower process. The actual reaction mechanism for U(V) removal by HCO_3^- remains to be understood.

■ ASSOCIATED CONTENT

Supporting Information

The Supporting Information is available free of charge at https://pubs.acs.org/doi/10.1021/acs.inorgchem.3c00682.

Details of the normalization of uranium dissolution experiments; full XPS scans of US 1−6; percents of different states of uranium in U $4f_{7/2}$ spectra deconvolution; discussion of U(VI) in U 4f spectra (PDF)

■ AUTHOR INFORMATION

Corresponding Author

Junyi Li − *Department of Chemistry, School of Engineering Sciences in Chemistry, Biotechnology and Health, KTH Royal institute of Technology, SE-10044 Stockholm, Sweden;* orcid.org/0000-0001-7099-2103; Email: ljunyi@kth.se

Authors

Xianjie Liu − *Laboratory of Organic Electronics, Department of Science and Technology, Linköping University, Norrköping SE-60174, Sweden;* orcid.org/0000-0002-3190-2774

Mats Jonsson − *Department of Chemistry, School of Engineering Sciences in Chemistry, Biotechnology and Health, KTH Royal institute of Technology, SE-10044 Stockholm, Sweden;* orcid.org/0000-0003-0663-0751

Complete contact information is available at: https://pubs.acs.org/10.1021/acs.inorgchem.3c00682

Author Contributions

Conceptualization: J.L. and M.J.; data curation: J.L.; formal analysis: J.L.; funding acquisition: M.J.; investigation: J.L. and X.L.; methodology: J.L. and M. J.; supervision: M.J.; writing − original draft J.L.; writing − review & editing: J.L., X.L., and M.J.

Funding

This work was supported by The Swedish Nuclear Fuel and Waste Management Company (SKB) [grant numbers 4501747777] and the China Scholarship Council (CSC) [grant number 201907930018].

Notes

The authors declare no competing financial interest.

■ ACKNOWLEDGMENTS

The Swedish Nuclear Fuel and Waste Management Company (SKB) and the China Scholarship Council (CSC) are gratefully acknowledged for financial support.

■ REFERENCES

(1) Suman, S. Hybrid Nuclear-Renewable Energy Systems: A Review. *J. Cleaner Prod.* **2018**, *181*, 166−177.

(2) Lankof, L. Assessment of Permian Zubers as the Host Rock for Deep Geological Disposal. *Energies* **2020**, *13*, 2239.

(3) Kleykamp, H. The Chemical State of the Fission Products in Oxide Fuels. *J. Nucl. Mater.* **1985**, *131*, 221−246.

(4) Ewing, R. C. Long-Term Storage of Spent Nuclear Fuel. *Nat. Mater.* **2015**, *14*, 252−257.

(5) Watson, N. *New IAEA Report Presents Global Overview of Radioactive Waste and Spent Fuel Management*; IAEA, https://www.iaea.org/newscenter/news/new-iaea-report-presents-global-overview-of-radioactive-waste-and-spent-fuel-management. 2022.

(6) Von Berlepsch, T.; Haverkamp, B. Salt as a Host Rock for the Geological Repository for Nuclear Waste. *Elements.* **2016**, *12*, 257−262.

(7) SKB *Design and Production of the KBS-3 Repository*; SKB, Technical Report. TR-10-12. 2010.

(8) Braden, Z.; Macfarlane, A. The Final Countdown to Site Selection for Canada's Nuclear Waste Geologic Repository. *Bull. At. Sci.* **2023**, *79*, 22−27.

(9) RWM. *Initial Evaluation Report: Theddlethorpe Gas Terminal Site and Surrounding Area within the East Lindsey Area*; RWM, 2021, 1−26.

(10) Vira, J. Geological Repository for High-Level Nuclear Waste Becoming Reality in Finland. *Geol. Repos. Syst. Safe Dispos. Spent Nucl. Fuels Radioact. Waste* **2017**, 645−666.

(11) Spinks, J. *An Introduction to Radiation Chemistry*; 3rd ed.; Wiley: New York, 1990.

(12) Ekeroth, E.; Roth, O.; Jonsson, M. The Relative Impact of Radiolysis Products in Radiation Induced Oxidative Dissolution of UO_2. *J. Nucl. Mater.* **2006**, *355*, 38−46.

(13) Nguyen-Trung, C.; Begun, G. M.; Palmer, D. A. Aqueous Uranium Complexes. 2. Raman Spectroscopic Study of the Complex Formation of the Dioxouranium(VI) Ion with a Variety of Inorganic and Organic Ligands. *Inorg. Chem.* **1992**, *31*, 5280−5287.

(14) Valérie Vallet, V.; Wahlgren, U.; Grenthe, I. Probing the Nature of Chemical Bonding in Uranyl(VI) Complexes with Quantum Chemical Methods. *J. Phys. Chem. A.* **2012**, *116*, 12373−12380.

(15) Li, J.; Szabó, Z.; Jonsson, M. Meta-Studtite Stability in Aqueous Solutions. Impact of HCO_3^-, H_2O_2 and Ionizing Radiation on Dissolution and Speciation. *Dalton Trans.* **2021**, *50*, 6568−6577.

(16) Zanonato, P. L.; Di Bernardo, P.; Szabó, Z.; Grenthe, I. Chemical Equilibria in the Uranyl(vi)-Peroxide-Carbonate System; Identification of Precursors for the Formation of Poly-Peroxometallates. *Dalton Trans.* **2012**, *41*, 11635−11641.

(17) Auque, L. F.; Gimeno, M. J.; Gomez, J. B.; Puigdomenech, I.; Smellie, J.; Tullborg, E. L. *Groundwater Chemistry around a Repository for Spent Nuclear Fuel over a Glacial Cycle: Evaluation for SR-Can*; SKB, 2006, 1−123.
(18) Jha, S.; Sinha, S.; Hazra, S. Hydrochemical Evolution and Assessment of Groundwater Quality in Fluorosis-Affected Area, Mandla District, Central India. *Groundwater Sustain. Dev.* **2021**, *14*, No. 100614.
(19) Turrero, M. J.; Buil, B.; Quejido, A.; Bajos, C. Hydrogeochemical Characteristics of Deep Groundwaters of the Hesperian Massif (Spain). *J. Iber. Geol* **2006**, *32*, 113−131.
(20) Burow, K. R.; Belitz, K.; Dubrovsky, N. M.; Jurgens, B. C. Large Decadal-Scale Changes in Uranium and Bicarbonate in Groundwater of the Irrigated Western U.S. *Sci. Total Environ.* **2017**, *586*, 87−95.
(21) Krishna Kumar, S.; Hari Babu, S.; Eswar Rao, P.; Selvakumar, S.; Thivya, C.; Muralidharan, S.; Jeyabal, G. Evaluation of Water Quality and Hydrogeochemistry of Surface and Groundwater, Tiruvallur District, Tamil Nadu. *India. Appl. Water Sci.* **2017**, *7*, 2533−2544.
(22) Sundin, S.; Dahlgren, B.; Roth, O.; Jonsson, M. H_2O_2 and Radiation Induced Dissolution of UO_2 and SIMFUEL in HCO_3^- Deficient Aqueous Solution. *J. Nucl. Mater.* **2013**, *443*, 291−297.
(23) Maier, A. C.; Kegler, P.; Klinkenberg, M.; Baena, A.; Finkeldei, S.; Brandt, F.; Jonsson, M. On the Change in UO_2 Redox Reactivity as a Function of H_2O_2 Exposure. *Dalton Trans.* **2020**, *49*, 1241−1248.
(24) Torrero, M. E.; Baraj, E.; De Pablo, J.; Giménez, J.; Casas, I. Kinetics of Corrosion and Dissolution of Uranium Dioxide as a Function of PH. *Int. J. Chem. Kinet.* **1997**, *29*, 261−267.
(25) De Pablo, J.; Casas, G.; Giménez, J.; Molera, M.; Rovira, M.; Duro, L.; Bruno, J. The Oxidative Dissolution Mechanism of Uranium Dioxide. I. The Effect of Temperature in Hydrogen Carbonate Medium. *Geochim. Cosmochim. Acta* **1999**, *63*, 3097−3103.
(26) El Jamal, G.; Gouder, T.; Eloirdi, R.; Jonsson, M. Monitoring the Gradual Change in Oxidation State during Surface Oxidation or Reduction of Uranium Oxides by Photoemission Spectroscopy of the 5f States. *J. Nucl. Mater.* **2022**, *560*, No. 153504.
(27) Maslakov, K. I.; Teterin, Y. A.; Popel, A. J.; Teterin, A. Y.; Ivanov, K. E.; Kalmykov, S. N.; Petrov, V. G.; Springell, R.; Scott, T. B.; Farnan, I. XPS Study of the Surface Chemistry of UO_2 (111) Single Crystal Film. *Appl. Surf. Sci.* **2018**, *433*, 582−588.
(28) Donald, S. B.; Dai, Z. R.; Davisson, M. L.; Jeffries, J. R.; Nelson, A. J. An XPS Study on the Impact of Relative Humidity on the Aging of UO_2 Powders. *J. Nucl. Mater.* **2017**, *487*, 105−112.
(29) Hansson, N. L.; Tam, P. L.; Ekberg, C.; Spahiu, K. XPS Study of External α-Radiolytic Oxidation of UO_2 in the Presence of Argon or Hydrogen. *J. Nucl. Mater.* **2021**, *543*, No. 152604.
(30) El Jamal, G.; Gouder, T.; Eloirdi, R.; Tereshina-Chitrova, E.; Horákd, L.; Jonsson, M. Mixed H_2O/H_2 Plasma-Induced Redox Reactions of Thin Uranium Oxide Films under UHV Conditions. *Dalton Trans.* **2021**, *50*, 12583−12591.
(31) Savvin, S. B. Analytical Use of Arsenazo III. *Talanta* **1961**, *8*, 673−685.
(32) Xing, W.; Yin, M.; Lv, Q.; Hu, Y.; Liu, C.; Zhang, J. Oxygen Solubility, Diffusion Coefficient, and Solution Viscosity. *Rotating Electrode Methods Oxyg. Reduct. Electrocatal.* **2014**, 1−31.
(33) Schindler, M.; Hawthorne, F. C.; Freund, M. S.; Burns, P. C. XPS Spectra of Uranyl Minerals and Synthetic Uranyl Compounds. I: The U 4f Spectrum. *Geochim. Cosmochim. Acta* **2009**, *73*, 2471−2487.
(34) Ilton, E. S.; Bagus, P. S. XPS Determination of Uranium Oxidation States. *Surf. Interface Anal.* **2011**, *43*, 1549−1560.
(35) Heisbourg, G.; Hubert, S.; Dacheux, N.; Purans, J. Kinetic and Thermodynamic Studies of the Dissolution of Thoria-Urania Solid Solutions. *J. Nucl. Mater.* **2004**, *335*, 5−13.
(36) Teterin, Y. A.; Popel, A. J.; Maslakov, K. I.; Teterin, A. Y.; Ivanov, K. E.; Kalmykov, S. N.; Springell, R.; Scott, T. B.; Farnan, I. XPS Study of Ion Irradiated and Unirradiated UO2 Thin Films. *Inorg. Chem.* **2016**, *55*, 8059−8070.
(37) Leinders, G.; Bes, R.; Pakarinen, J.; Kvashnina, K.; Verwerft, M. Evolution of the Uranium Chemical State in Mixed-Valence Oxides. *Inorg. Chem.* **2017**, *56*, 6784−6787.
(38) Walshe, A.; Prüßmann, T.; Vitova, T.; Baker, R. J. An EXAFS and HR-XANES Study of the Uranyl Peroxides [UO2(η 2-O2)(H2O)2]·nH2O (n = 0, 2) and Uranyl (Oxy)Hydroxide [(UO2)4O(OH) 6]·6H2O. *Dalt. Trans.* **2014**, *43*, 4400−4407.
(39) Kvashnina, K. O.; Kowalski, P. M.; Butorin, S. M.; Leinders, G.; Pakarinen, J.; Bès, R.; Li, H.; Verwerft, M. Trends in the Valence Band Electronic Structures of Mixed Uranium Oxides. *Chem. Commun.* **2018**, *54*, 9757−9760.
(40) Li, J.; Maier, A. C.; Jonsson, M. Stability of Studtite in Aqueous Suspension: Impact of HCO_3^- and Ionizing Radiation on the Dynamics of Dissolution. *ACS Appl. Energy Mater.* **2020**, *3*, 352−357.
(41) Gorman-Lewis, D.; Burns, P. C.; Fein, J. B. Review of Uranyl Mineral Solubility Measurements. *J. Chem. Thermodyn.* **2008**, *40*, 335−352.
(42) Vitova, T.; Pidchenko, I.; Biswas, S.; Beridze, G.; Dunne, P. W.; Schild, D.; Wang, Z.; Kowalski, P. M.; Baker, R. J. Dehydration of the Uranyl Peroxide Studtite, [UO2(N2-O2)(H2O)2]·2H2O, Affords a Drastic Change in the Electronic Structure: A Combined X-Ray Spectroscopic and Theoretical Analysis. *Inorg. Chem.* **2018**, *57*, 1735−1743.
(43) Dos Reis, R. D.; Veiga, L. S. I.; Escanhoela, C. A.; Lang, J. C.; Joly, Y.; Gandra, F. G.; Haskel, D.; Souza-Neto, N. M. Unraveling 5f-6d Hybridization in Uranium Compounds via Spin-Resolved L-Edge Spectroscopy. *Nat. Commun.* **2017**, *8*, 1203.
(44) Havela, L.; Paukov, M.; Dopita, M.; Horak, L.; Cieslar, M.; Drozdenko, D.; Minarik, P.; Turek, I.; Divis, M.; Legut, D.; Kyvala, L.; Gouder, T.; Huber, F.; Seibert, A.; Tereshina-Chitrova, E. XPS, UPS, and BIS Study of Pure and Alloyed β-UH_3 Films: Electronic Structure, Bonding, and Magnetism. *J. Electron Spectros. Relat. Phenomena.* **2020**, *239*, No. 146904.
(45) Liu, N.; He, H.; Noël, J. J.; Shoesmith, D. W. The Electrochemical Study of Dy2O3 Doped UO2 in Slightly Alkaline Sodium Carbonate/Bicarbonate and Phosphate Solutions. *Electrochim. Acta* **2017**, *235*, 654−663.
(46) Razdan, M.; Shoesmith, D. W. The Influence of Hydrogen Peroxide and Hydrogen on the Corrosion of Simulated Spent Nuclear Fuel. *Faraday Discuss.* **2015**, *180*, 283−299.
(47) Zhu, Z.; Noël, J. J.; Shoesmith, D. W. Hydrogen Peroxide Decomposition on Simulated Nuclear Fuel Bicarbonate/Carbonate Solutions. *Electrochim. Acta* **2020**, *340*, No. 135980.
(48) Wu, L.; Shoesmith, D. W. An Electrochemical Study of H2O2 Oxidation and Decomposition on Simulated Nuclear Fuel (SIMFUEL). *Electrochim. Acta* **2014**, *137*, 83−90.
(49) Zhu, Z.; Wu, L.; Noël, J. J.; Shoesmith, D. W. Anodic Reactions Occurring on Simulated Spent Nuclear Fuel (SIMFUEL) in Hydrogen Peroxide Solutions Containing Bicarbonate/Carbonate − The Effect of Fission Products. *Electrochim. Acta* **2019**, *320*, 134546.
(50) Broczkowski, M. E.; Noël, J. J.; Shoesmith, D. W. The Influence of Dissolved Hydrogen on the Surface Composition of Doped Uranium Dioxide under Aqueous Corrosion Conditions. *J. Electroanal. Chem.* **2007**, *602*, 8−16.
(51) Liu, N.; King, F.; Noël, J. J.; Shoesmith, D. W. An Electrochemical and Radiolytic Study of the Effects of H2 on the Corrosion of UO2-Based Materials. *Corros. Sci.* **2021**, *192*, No. 109776.
(52) Goldik, J. S.; Nesbitt, H. W.; Noël, J. J.; Shoesmith, D. W. Surface Electrochemistry of UO2 in Dilute Alkaline Hydrogen Peroxide Solutions. *Electrochim. Acta* **2004**, *49*, 1699−1709.
(53) Ulrich, K. U.; Ilton, E. S.; Veeramani, H.; Sharp, J. O.; Bernier-Latmani, R.; Schofield, E. J.; Bargar, J. R.; Giammar, D. E. Comparative Dissolution Kinetics of Biogenic and Chemogenic Uraninite under Oxidizing Conditions in the Presence of Carbonate. *Geochim. Cosmochim. Acta* **2009**, *73*, 6065−6083.
(54) Kern, D. M. H.; Orlemann, E. F. The Potential of the Uranium (V), Uranium (VI) Couple and the Kinetics of Uranium (V)

Disproportionation in Perchlorate Media1,2. *J. Am. Chem. Soc.* **1949**, *71*, 2102−2106.

(55) Yuan, K.; Renock, D.; Ewing, R. C.; Becker, U. Uranium Reduction on Magnetite: Probing for Pentavalent Uranium Using Electrochemical Methods. *Geochim. Cosmochim. Acta* **2015**, *156*, 194−206.

(56) Du, J.; Douair, I.; Lu, E.; Seed, J. A.; Tuna, F.; Wooles, A. J.; Maron, L.; Liddle, S. T. Evidence for Ligand-and Solvent-Induced Disproportionation of Uranium(IV). 2021, *12*, 4832, DOI: 10.1038/s41467-021-25151-z.

(57) Hoekstra, H. R.; Siegel, S. The Uranium-Oxygen System: U3O8-UO3. *J. Inorg. Nucl. Chem.* **1961**, *18*, 154−165.

(58) Miskowiec, A.; Spano, T.; Hunt, R.; Shields, A. E.; Niedziela, J. L.; Finkeldei, S. Structural Features of Solid-Solid Phase Transitions and Lattice Dynamics in U3 O8. *Phys. Rev. Mater.* **2020**, *4*, No. 093610.

https://doi.org/10.1021/acs.inorgchem.3c00682
Inorg. Chem. 2023, 62, 7413−7423